Spatial variability of liquid water path in marine low cloud: Part II. Climatology and dependence upon large-scale parameters.

ROBERT WOOD* and DENNIS. L. HARTMANN

University of Washington, Seattle, Washington

April 14, 2004

**Corresponding author address:* Dr. Robert Wood, Atmospheric Sciences, University of Washington, Seattle, WA; *e-mail: robwood@atmos.washington.edu.*

Abstract

In part I of this study we focused upon models to describe the mesoscale spatial variability of cloud liquid water path LWP is low cloud. Here, we construct simple, exploratory, climatologies of the spatial variability characteristics of marine low clouds for two regions of the East Pacific. The climatologies show interesting and important geographical variability. Large scale meteorological conditions are assessed for each MODIS scene using NCEP/NCAR reanalysis data, and regression analysis is used to assess relationships between large-scale forcings and mesoscale variability. Cloud fraction and homogeneity are both strongly modulated by lower tropospheric stability LTS on timescales of days to weeks. While marine boundary layer (MBL) depth z_i is itself modulated strongly by LTS, cloud fraction is not found to correlate well with z_i, suggesting that it is LTS itself, rather than z_i that is the primary determinant of low cloud fraction. However, MBL thermodynamic and cloud mesoscale variability appears to be controlled by z_i. This result reflects the findings that mesoscale variability is an increasing function of the characteristic lengthscale of the mesoscale cellular convection (MCC), and that the characteristic lengthscale scales with z_i. The observed changes in cloud mesoscale variability from shallow stratus-topped MBLs through to trade cumulus can be accounted for using a physical framework that links MBL thermodynamic variability and cloud liquid water path variability using a pdf formulation. The pdf width is strongly tied to the MBL depth, and it is suggested that this framework, with scalings constrained by observations, is suitable for the parameterization of low cloud subgrid spatial variability in large-scale numerical models.

1. Introduction

Spatial variability in marine boundary layer (MBL) low cloud is ubiquitous and is important both radiatively and dynamically (Cahalan et al. 1994; Rossow et al. 2002; Pincus and Klein 2000; Rotstayn 2000; Larson et al. 2001; Wood et al. 2002). Despite this importance, so far only limited attempts have been made to systematically quantify this variability over large regions of the oceans on timescales appropriate to large-scale numerical modeling, and the attempts that have been made tend to aggregate the effects of all cloud types (e.g. Rossow et al. 2002).

In Part I of this study we presented a method to break Moderate Resolution Imaging Spectroradiometer (MODIS) liquid water path data into 256×256 km "scenes" to which we then apply a number of analysis tools including probability density function (pdf) and power spectral analysis. We found that three variables (mean cloud-only liquid water path $\overline{LWP}$, cloud fraction CF, and the square of the ratio of the mean to standard deviation of cloud-only liquid water path γ_{LWP} provide a fairly complete description of the one point LWP statistics in MBL clouds. We also found that a simple Gaussian model of the saturation excess pdf (or, equivalently cloud thickness pdf) is quite successful at modeling the relationship between CF and cloud liquid water path variability. This model ties together the thermodynamic and cloud structure of the MBL in a way that may be suitable for parameterization in large-scale numerical models (see e.g. Park et al. 2004, which adopts an identical pdf form).

In Part II of this study, we continue our investigation into spatial variability in marine low cloud using MODIS. We focus here upon simple climatologies of the spatial variability characteristics for two regions of the East Pacific Ocean (see Part I for details of the regions studied). In addition, we extend our analysis using data from the NCEP/NCAR reanalysis, which allows an investigation

of the relationships between mesoscale spatial variability and associated large-scale forcings. We also examine a scaling between mesoscale cellular convection (MCC), spatial variability and MBL depth which may prove to be useful in the parameterization of mesoscale spatial variability and CF in MBL clouds.

2. Datasets used

Data used in this study are detailed in Part I, and only a brief description is given here. We use 1 km (at nadir) pixel data from the Moderate Resolution Imaging Spectroradiometer (MODIS) on the NASA Terra polar-orbiting sun-synchronous satellite. We estimate liquid water path LWP from the $r_{e,top}$ and τ level 2 cloud product, and this is the primary dataset analysed. Only daytime ($\sim$ 10:30 LST) scenes containing exclusively warm cloud are analysed. All available MODIS data from September and October 2000 are used.

MBL depth z_i is estimated using the method presented in Wood and Bretherton (2003), a novel technique that uses cloud top and sea surface temperature, cloud liquid water path, and the simple model of Park et al. (2004) to determine z_i and the degree of decoupling in the MBL. Estimates of the accuracy of this techinique suggest that the uncertainty in each z_i estimate is approximately 200-300 m (Wood and Bretherton 2003).

Reanalysis data from NCEP/NCAR (Kistler et al. 2001) are used to investigate links between large-scale meteorology and mesoscale spatial variability. Our methodology is to obtain a set of pertinent reanalysis variables for each of the MODIS scenes analysed. Reanalysis data are available four times daily on a 2.5×2.5° grid, and include sea surface temperature data (Reynolds and Smith 1994). Trilinear interpolation is used to determine the values of the reanalysis variables at the MODIS scene-center locations and times. We consider three large-scale variables derived

from reanalysis in this study: lower tropospheric stability ($LTS = \theta_{700hPa} - \theta_0$, where θ is potential temperature); large-scale vertical motion at 850 hPa (w_{850}); temperature advection $\mathbf{U} \cdot \nabla SST$. Because it is known that there exists a sizeable diurnal cycle in surface divergence and subsidence rates above the MBL (Dai and Deser 1999), we use the mean w_{850} for the 24 hour period centered on the time of the MODIS overpass. This is unnecessary for the other reanalysis parameters as their diurnal cycles are much weaker.

3. Climatology of mesoscale variability

Two month means (September/October 2000) using the MODIS data are used show geographical variations in the cloud mesoscale variability parameters. Data are binned into 2.5×2.5° regions to produce maps. The number of MODIS scenes contributing to each 2.5×2.5° average for the two month period is between 10 and 60.

a. LWP pdf parameters

Median values of $\overline{LWP}$ (mean LWP of cloudy fraction) range from around 40 g m^{-2} to 80 g m^{-2} (Fig. 1(a,b)). In the NE Pacific, $\overline{LWP}$ increases slightly, from around 40-50 g m^{-2} in the stratus regions near the Californian coast, to around 60 g m^{-2} in the trade wind regions. The trend is similar in the SE Pacific, with low values close to the Chilean coast, increasing downwind. However, $\overline{LWP}$ tends to decrease again in the SE Pacific trade winds. A general feature (not shown) is that in regions with high climatological cloud fraction ($\overline{CF} > 0.6$), $\overline{LWP}$ is positively correlated with CF, whereas there is little correlation for regions where the mean CF is lower.

Maps of CF and γ_{LWP} (Fig. 1(c-f)) demonstrate the strong connection between these parameters examined in part I. The most homogeneous LWP (and the highest CF) is found along the Californian and Chilean coasts, and decreases towards the remote ocean and trade-wind regions. The coverage of both unbroken (e.g. $CF > 0.6$) and homogeneous cloud (e.g. $\gamma_{LWP} > 2$) is more extensive in the SE than in the NE Pacific during this season. A longer dataset is required to determine whether the $CF - \gamma_{LWP}$ links exist on seasonal timescales, and thereby be useful for parameterizing unresolved variability in climate models. The clouds remain unbroken and homogeneous into the SE Pacific tropical equatorial region, quite unlike the situation in the NE Pacific, reflecting differences in the SST patterns and prevailing winds in the two regions. Stronger cold advection in the NE Pacific stratocumulus region most likely hastens the decoupling process and rate of MBL deepening by increasing surface fluxes. Figure 2 shows mean z_i for September/October 2000. MBLs originating close to the Chilean coast deepen far less rapidly (in the Lagrangian sense) than comparable MBLs in the NE Pacific as they advect equatorwards. Therefore, the effect of MBL deepening upon decoupling Bretherton and Wyant (1997) may be of reduced importance in the SE Pacific. There is evidence that mean entrainment rates in the region of maximum cloud cover in the SE Pacific are lower than those in the corresponding region of the NE Pacific (Wood and Bretherton 2003) which would reduce the MBL deepening there.

b. Characteristic lengthscale

Figure 3 shows maps of the median characteristic cell size λ_1. We only include scenes with $CF > 0.2$ because obtaining λ_1 from low CF scenes is more uncertain. The smallest cells (< 20 km) are found over the cold water close to the Oregon/Californian coast, with a strong oceanward gradient. Cell sizes reach a maximum of around 40-45 km as the subtropical airmass advects over warmer

waters and the MBL deepens. SE Pacific values show a somewhat similar trend with the smallest values associated with regions of climatologically shallow MBLs (see Fig. 2). As in the NE Pacific, cell sizes reach around 40-45 km in the trades. Links between cell size, thermodynamic variance and MBL depth are explored in Section 5.

c. Homogeneous, open or closed mesoscale cellular convection?

Figure 4 shows a climatology of the prevalence of homogeneous cloud (no MCC), closed MCC, open MCC, and heterogeneous cloud without clear MCC, using the method described in Part I. Homogeneous clouds are rare apart from north of 40N, along the Californian/Baha coastline, and close to the Chilean coasts, all regions with the shallowest MBLs (Fig. 2). Closed and open MCC is very common over much of the NE and SE Pacific but is relatively more common in the SE Pacific during this season. Closed MCC is common just to the north of the equatorial region out to 120W, Open MCC becomes prevalent over the warmer water trade-wind regions of the SE and NE Pacific, and to the north of the equatorial cold tongue. The diagnosis of open MCC also tends to include heterogeneous mesoscale rolls that seem to be peculiar to the region north of the equatorial cold tongue. It should be noted that it is perhaps inappropriate to classify these rolls as open MCC, but further subclassification of the groups was not attempted in this study. Heterogeneous scenes with no clear MCC are common over warmer waters, and in the NE Pacific in general, during this season. It will be interesting to examine the seasonality of these cloud types using an extended dataset.

The transition (in a Lagrangian sense) from homogeneous, through closed and then open MCC regions can be conceptualized as the stratocumulus to cumulus transition (SCT, Bretherton and

Pincus 1995; Bretherton et al. 1999; de Roode and Duynkerke 1997), with the most homogeneous clouds being stratus, the closed MCC being stratocumulus, and the open MCC being more cumuliform.

4. The influence of large-scale parameters

Klein (1997) demonstrates that both LTS and temperature advection (cold advection positive) are positively correlated with nighttime low cloud amount at ocean weather station November (30N, 140W) in the subtropics. Our data also support these general findings, although in this study we focus additionally upon the large-scale influence upon parameters related to the spatial variability in low cloud fields - $\overline{LWP}$, γ_{LWP} and the characteristic length scale λ_1.

a. Regression maps of daily data

Maps showing the regression of cloud-mean liquid water path $\overline{LWP}$, CF, and homogeneity parameter γ_{LWP} onto large scale parameters are shown in Figs. 5 ($\overline{w_{850}}$), 6 (LTS), and 7 (temperature advection). Regressions were performed by first averaging the data from all the MODIS scenes in a 5×5° resolution grid for each day to create a daily timeseries at each gridbox. Not all days at each location contain data but this is not important for regression analysis.

The cloud-mean LWP is influenced strongly by $\overline{w_{850}}$ in the NE Pacific stratocumulus region, especially close to the Californian coast, with positive anomalies in 850 hPa vertical wind (reduced subsidence) associated with increased $\overline{LWP}$. Little effect is observed elsewhere, except in the trade-wind and tropical regions of the SE Pacific, where a similar correlation is found. Vertical wind is uncorrelated with cloud fraction everywhere, and only weakly correlated with γ_{LWP} off

the Baha peninsula, where increased subsidence favors more homogeneous cloud.

LTS is found to be uncorrelated with $\overline{LWP}$ in the NE Pacific, and only for a small region of the SE Pacific. However, LTS is strongly correlated with CF in both the NE and SE Pacific subtropical regions, particularly those with large climatological cloud fraction. This correlation, which has been explored in previous work (e.g. Slingo 1980, 1987; Klein and Hartmann 1993; Klein 1997) forms the basis for the parameterization of low cloud in a number of large-scale numerical models. Klein and Hartmann (1993) show that the relationship between LTS and CF is remarkably strong on seasonal timescales and over large regions. The evidence in Fig. 6 suggests that this relationship exists on scales of days to weeks, and on quite small geographical scales. However, this correlation becomes much weaker in the trade-wind regions, but this may be in part because the degree of day-to-day variability in both cloud amount and LTS in the trade wind regions is much weaker. A longer time record of daily data is required to establish whether the $CF - LTS$ correlations truly disappear on daily to weekly timescales in the trade-wind regions.

Another surprise is that in the SE Pacific, the correlation becomes small in the region east of 100W and north of 15S (coastal Peruvian region), which is a region dominated by stratocumulus clouds. Indeed, CF is found to be uncorrelated with any of the large scale parameters (or MBL depth) in this region. Why this should be is unclear, but it might be useful to speculate on possible causes. First, in this region both the CF variability and LTS are markedly smaller than anywhere to the south and west, and anywhere in the NE Pacific stratocumulus region (Fig. 8). This is likely related to the moderating influence of the Andes mountains on the tropospheric temperatures over the far Eastern Pacific. Thus, even if LTS and CF are related in this region, it is easier for additional physical factors (or noise) to drown out signals in the regressions. Free-tropospheric moisture does not correlate with CF in this region (no significant correlations with CF are found

anywhere in the NE or SE Pacific, except to the north of the equatorial cold tongue). Second, the lack of clear controlling factors for cloud amount could hint at an internal source for CF variability in the coastal Peruvian region, which might involve aerosol-drizzle-cloud feedbacks. This is difficult to investigate with the current dataset, because effective radius retrievals are known to be biased in regions of broken, inhomogeneous cloud (Graeme Stephens, personal communication), and thus spurious correlations between these two variables are likely to arise.

In order to be consistent with the Gaussian-s model, increased LTS should increase γ_{LWP} together with CF, and increased $\overline{w_{850}}$ should not be correlated with γ_{LWP}. This is indeed the case in the regions with marked $LTS - CF$ correlations (Figs. 6(e,f)).

Temperature advection (Fig. 7) is only weakly correlated with $\overline{LWP}$, but is quite well correlated with CF, particularly in the stratocumulus to cumulus transition region of the NE Pacific (as found in Klein 1997), in the stratocumulus regions south of 20S, and to the north of the equatorial cold tongue, where particularly strong cold advection results in strong surface forcing (deSzoeke and Bretherton 2004), and tropical instability waves provide important modulation of the surface fluxes (Thum et al. 2002).

Fig. 9 demonstrates that z_i has very little correlation with $\overline{LWP}$, and only weak correlation with CF. This is surprising given that the patterns of geographical variability in mean CF (Fig. 1) and MBL depth (Fig. 2) are remarkably similar. LTS and z_i are strongly negatively correlated (r=-0.4 to -0.7) in the regions where LTS and CF are strongly positively correlated (Fig. 10), which makes the lack of $z_i - CF$ correlation in these areas all the more puzzling. Although MBL depth is clearly influenced by LTS on daily-weekly timescales, it does not appear to be the z_i fluctuations themselves that are modulating CF. The cloud homogeneity γ_{LWP} is found to negatively correlate with z_i, especially over the NE Pacific, suggesting that while z_i may not be the primary modulator

of CF, it may influence the mesoscale variability.

In the NE Pacific there is a large region where MBL depth and γ_{LWP} are negatively correlated. In the SE Pacific, this correlation is small apart from at the south of the region. The MBL depth appears to have a generally larger influence upon cloud homogeneity on the short timescale than it does upon the cloud amount, particularly in the NE Pacific. This may be because thermodynamic and cloud inhomogeneity is closely tied to the characteristic lengthscale of mesoscale cells, which is well correlated with z_i, particularly in the regions of extensive stratocumulus clouds (not shown). We return to this scaling of mesoscale features with MBL depth in Section 5.

To assess the key driving force for the modulation of clouds and large scale forcings on daily to monthly timescales, we use autocorrelation analysis on the daily timeseries for each $5\times5^\circ$ gridbox. Standard harmonic analysis is precluded because each gridbox does not contain data on every day during the analysis period. Autocorrelation data are obtained for each series at lags of 1-30 days, and for each series with at least 50% of the maximum possible data points we estimate the non-zero lag at which the series becomes best correlated again with itself. This lag is the dominant timescale and coincides with the period of the dominant mode of variability. This timescale is plotted in Fig. 11 as a function of latitude. Several key points are noted. First, the dominant timescales are mostly in the range 7-12 days and do not vary strongly with latitude. Spectral analysis of midlatitude geopotential fields reveals a dominant mode of variability with an approximate 10 day period (Fraedrich and Bottger 1978) corresponding to eastward propagating long waves. Hakim (2003) demonstrates that these waves are, in fact, midlatitude wave packets forming in the North Pacific storm track, and that they frequently penetrate deep into the subtropics, and sometimes the tropics. Second, the timescales of cloud and forcing parameters are approximately equal confirming that the variability in subtropical clouds on daily to weekly timescales is governed largely by variability

in baroclinic forcing. The lack of strong latitudinal trends in the dominant timescale of the forcing parameters suggests that the effects of baroclinic instability is probably the most important driver of the variability of subtropical clouds on daily to monthly timescales.

b. Geographical variation of means

Geographical variations of the mean large-scale parameters corresponding to the MODIS scenes are shown in Fig. 12. Subsidence is a typical feature of the MBL cloud cases throughout most of the NE and SE Pacific regions, but MBL clouds are also found in regions of large-scale ascent, most notably in the ITCZ regions at latitudes of 5-15N. There also appears to be strongly reduced subsidence, and even ascent, close to the northern Chilean coast, which may be related to a mountain-influenced sea-breeze structure (Garreaud and Muñoz 2004), although it cannot be ruled out as an artifact of the reanalysis data upstream of strongly sloping terrain. Strong lower LTS prevails in the eastern Pacific regions, particularly over the coastal upwelling regions of the subtropics. Temperature advection is largely positive (i.e. cold advection) throughout the two regions, apart from very close to the northwestern United States coastline and along the equatorial cold tongue. Very strong cold advection is observed to the north of the cold tongue as cool air flows northwards over a strong gradient in sea surface temperature.

Geographical variations of climatological mean CF as a function of both LTS and MBL depth are examined on the longer two monthly timescale using the $2.5\times2.5^\circ$ means (Figure 13). We only include SE Pacific data south of the equator where the surface forcing is relatively weak. In addition, we should emphasize that the mean cloud amounts discussed here are the mean values for the daytime (10:30 am local time) MODIS overpasses. Given that diurnal maxima in CF and

mean liquid water path occurs typically at 3-6 am (Rozendaal et al. 1995; Wood et al. 2002), the MODIS cloud amounts (measured ∼6 hours after the peak) are fairly representative of the diurnal mean cloud amount.

There is a tight correlation between mean LTS and CF (r=0.86 and 0.90 for the NE and SE Pacific subtropical regions) which holds through the entire range of mean cloud amounts observed (∼0.2 to ∼0.9). The best fit is close to that found for the climatological mean cloud amounts for a number of regions (Klein and Hartmann 1993), although we find the sensitivity of the mean cloud amount to the LTS to be 20% greater. Correlations between mean CF and z_i are almost as high as for LTS (0.81 and 0.87 for the NE and SE Pacific respectively), which is surprizing given the lack of regression on short timescales between these parameters. Data from regions where little correlation exists on the short timescales (such as the coastal Peruvian region discussed above) fall onto the well-correlated spread in data, suggesting that low variability may be primarily responsible for the poor daily correlations in these regions. However, in regions where LTS is well correlated with CF and z_i, reduced variability is not responsible for the poor $z_i - CF$ correlations.

c. What controls cloud fraction and homogeneity?

Reduced variability cannot entirely explain why the climatological coupling between z_i and CF is so tight and yet the daily correlations are so small. Two hypotheses for why increasing LTS tends to increase the cloud amount both center around the idea that increased LTS results in reduced entrainment rates because greater work must be done to overcome greater stratification:

(i) reduced entrainment associated with greater LTS leads to shallower MBLs. Shallower MBLs are more likely to remain well-mixed (Bretherton and Wyant 1997) so that the cloud layer

remains connected to the oceanic moisture supply. Deeper MBLs on the other hand are more likely to decouple, and this decoupling results in cloud breakup;

(ii) reduced entrainment associated with greater LTS entrainment prevents the incorporation of warm, dry air into the MBL. A cooler, moister boundary layer is more favourable for the maintenance of cloud.

On the seasonal mean timescale it appears that hypothesis (i) is supported by the data, with the largest mean CFs being associated with the greatest LTS and shallowest MBLs. However, the local regression analysis suggests that (i) is not supported by the data because of the lack of good correlation between z_i and CF. This suggests the tentative conclusion that although increased LTS is associated with shallow z_i, it is LTS itself, rather than the MBL depth *per se* that controls the cloud cover. This leaves the possibility that hypothesis (ii) is the most important effect of increased LTS. However, there is no available data at present to examine this relationship on the daily timescale because we do not have entrainment estimates at this high time resolution. We hope that an extensive Lagrangian-type analysis of high temporal resolution GOES data may be able to address this hypothesis on short timescales.

5. Scaling of mesoscale variability

Figure 14 shows the median characteristic cell lengthscale λ_1 binned as a function of MBL depth z_i. When the MBL depth is greater than ∼ 600 m, the cells tend to organize with preferred aspect ratios (horizontal:vertical cell scale) in the range 30-40. There is considerable variation of this aspect ratio from scene to scene, as might be expected if some considerable time is required for cells to equilibrate at their preferred scale (see e.g. Shao and Randall 1996). For example, for MBLs between 1200-1300 m deep, the 25th, 50th and 75th percentiles of λ_1 are 31, 41 and 63 km

respectively, indicating a considerable range within each z_i class. However, it is possible that this spread is caused by random errors and ambiguity in the determination of λ_1 from the MODIS scenes. It could also be caused by the MCC growth timescale being comparable or longer than the MBL growth timescale. Lagrangian studies of evolving MCC using geostationary satellites may prove to be a useful tool to resolve these issues. The relation $\lambda_1 = 4.6(z_i - 550)^{1/3}$ (z_i in m and λ_1 in km) fits the data quite well and is shown in Fig. 14.

For z_i lower than $\sim$ 800 m there is a marked decrease in λ_1 suggesting that the growth of MCC is not favored in well-mixed shallow MBLs. Indeed, for $z_i < 600$ m MCC is seldom observed in our dataset. This provides some support for the conceptual model proposed by Shao and Randall (1996) whereby the production of MCC requires the presence of a stable layer in the middle of the cloud-topped MBL. Such stable layers are associated with the decoupling of the MBL, a phenomenon rarely observed when $z_i < 600$ m or so. It is hypothesized that the presence or absence of MCC might be a sensitive indicator of MBL decoupling. To be tested, this speculation would require additional investigation with a combination of satellite and in-situ data. Synthetic aperture radar can readily detect patterns of variability in surface wind that correspond to MCC in cold air outbreaks. The presence or absence of such patterns in subtropical MCC may be a sensitive indicator of MBL decoupling, and is worthy of investigation.

An automatic classification procedure described in Part I allows us to determine the scenes containing MCC, and for these scene, whether the MCC is of open or closed type. With this classification we find that the $\lambda_1 - z_i$ relationships for open and for closed cells are very similar when $z_i > 800$ m (not shown). However, closed cells are much the commoner type of MCC when the MBL is shallower (constituting 83% of the MCC scenes when $800 < z_i < 1200$, but only 38% in MBLs deeper than 2000 m). From this we hypothesize that the cell scale is not determined

by whether the MCC is open or closed, but that open MCC becomes more favorable in deeper MBLs. Although the Shao and Randall conceptual model for closed MCC may indeed be driven by cloud top radiative cooling, it is difficult to account for open MCC with this mechanism. This leads one to wonder if it is purely coincidental that there appears to be no systematic difference between the median aspect ratios in open and closed MCC. Or, is a single mechanism responsible for the generation of the two types of MCC? Large eddy simulations (de Roode et al. 2004) with extensive domains suggest that radiative cooling is not necessary for the generation of MCC (see also the introduction of Part I of this study). Instead, particular configurations of the buoyancy flux profile lead to mesoscale fluctuations. Such profiles may be caused by latent heating and drizzle, in addition to radiative cooling.

The MCC characteristic lengthscale λ_1 is an important parameter because it is closely tied to the degree of mesoscale variance in saturation excess. In Part I a method was presented to estimate the standard deviation of the saturation excess σ_s in the cloud layer, using MODIS observations of the LWP pdf. In Figure 15 we show plots of median σ_{LWP} and median estimated σ_s against cell scale λ_1 and MBL depth z_i. Both σ_{LWP} and σ_s increase as λ_1 increases, indicating that enhanced mesoscale variance in relative humidity and consequently LWP is associated with larger cells. Near-linear relationships are found between $\sigma_{LWP} - z_i$ and $\sigma_s - z_i$. Also shown are median values from a number of intensive field programs (Wood and Taylor 2001; Wood et al. 2002; Bretherton et al. 2003) in subtropical MBLs in the NE Atlantic (ASTEX), NE Pacific (FIRE) and SE Pacific (EPIC). Aircraft observations and microwave radiometer LWP are derived from reliable measurements and provide support that a general scaling exists between mesoscale variability and MBL depth, and is intimately coupled through the mechanism of MCC cell growth.

6. Discussion and conclusions

In Part II of this study we have presented an initial attempt at producing a climatology of low cloud mesoscale variability over the NE and SE Pacific Ocean, using 1 km resolution data from MODIS. We have used a number of parameters, discussed in more depth in Part I of the study, that best characterize the mesoscale spatial variability in MBL cloud. We find that three parameters (CF, mean in-cloud liquid water path, and the square of the ratio of the mean to standard deviation of the cloud-only liquid water path) provide a reasonably complete description of the one point statistics of cloud liquid water path mesoscale spatial variability. We also find that cloud homogeneity is strongly coupled with CF, and that the spatial variability in cloud can be coupled quite effectively to variability in the underlying thermodynamic parameters using a simple Gaussian model of saturation excess.

In Part II, we have examined how these parameters vary in relation to large-scale forcings from NCEP reanalysis products, using both regressions of daily gridded data and by examining the geographical variability of mean values. The results suggests that both cloud cover and the mesoscale spatial variability within cloud are modulated by fluctuations in forcing variables, particularly LTS (Klein and Hartmann 1993) and temperature advection (Klein 1997). In many places, most notably off the coast of Peru, cloud cover and spatial variability does not correlate strongly with any of the forcing variables examined, but this may be because the daily to monthly variability is very low.

While there are very good relationships between 2.5×2.5° means of CF and both LTS and MBL depth, the regression analysis shows that CF variations are not strongly correlated with z_i. This suggests that it may be variation in entrainment rate, rather than z_i *per se* that controls the cloud fraction.

Cloud homogeneity γ_{LWP} correlates with z_i in regions where the $CF - z_i$ correlations are poor, suggesting that the mesoscale variability may indeed be more strongly controlled by MBL depth than entrainment rate. The observed couplings between mesoscale LWP/saturation excess variance, the characteristic lengthscale of the mesoscale cellular convection (MCC), and the MBL depth, are good evidence that there may exist well-defined scalings between the MBL depth and the thermodynamic/cloud spatial variability properties in the MBL. These may be useful, both in offering insight into the processes controlling mesoscale spatial variability in MBL clouds, and for future development of parameterizations to account for such variability.

Finally, we can demonstrate schematically how the transition from shallow stratus-topped MBLs through stratocumulus to the deeper trade-wind MBLs occurs in the context of the Gaussian model linking saturation excess and cloud properties (Fig. 16). As we discussed in Part I of this study, we can represent the observed cloud mesoscale properties ($\overline{LWP}$, CF, γ_{LWP}) by assuming a Gaussian distribution of saturation excess and a locally adiabatic model. Equivalently, this can be conceptualized using a Gaussian pdf of the LCL and an adiabatic profile for $z < z_i$, with no cloud in the fractional area where $LCL > z_i$. The evolution of the clouds and their mesoscale structure along equatorward trajectories can be conceptualized as a rising of z_i, a more rapid rising of the mean LCL, and an increase in the width of the pdf of the LCL (or saturation excess). In part I, we saw that the the mean LWP is roughly conserved in the transition from stratus to trade cumulus, and we suggested that this may be related to active feedbacks, possibly involving drizzle and longwave radiation. The climatology of $\overline{LWP}$ (Fig. 1) confirms this relatively narrow range of $\overline{LWP}$. The evolution of the LCL pdf (or equivalently the saturation deficit pdf) provides a theoretical framework for the observed changes in the mesoscale variability of clouds in the subtropics. Recent advances in the parameterization of cloud-topped MBLs (e.g. Martin et al. 2000) diagnose

MBL depth, and this could be used to parameterize the saturation excess pdf width, thereby accounting for unresolved subgrid variability in cloud structure (Fig. 15) in a physically consistent manner.

References

Bretherton, C. S., S. K. Krueger, M. C. Wyant, P. Bechtold, E. vanMeijgaard, B. Stevens, and J. Teixeira: 1999, A gcss boundary layer model intercomparison study of the first astex lagrangian experiment. *Bound. Layer Meteorol.*, **93**, 341–380.

Bretherton, C. S. and R. Pincus: 1995, Cloudiness and marine boundary layer dynamics in the ASTEX lagrangian experiments. Part I: Synoptic setting and vertical structure. *J. Atmos. Sci.*, **52**, 2707–2723.

Bretherton, C. S., T. Uttal, C. W. Fairall, S. E. Yuter, R. A. Weller, D. Baumgardner, K. Comstock, and R. Wood: 2003, The EPIC 2001 stratocumulus study. *Bull. Am. Meteorol. Soc.*, in review.

Bretherton, C. S. and M. C. Wyant: 1997, Moisture transport, lower-tropospheric stability, and decoupling of cloud-topped boundary layers. *J. Atmos. Sci.*, **54**, 148–167.

Cahalan, R. F., W. Ridgway, W. J. Wiscombe, T. L. Bell, and J. B. Snider: 1994, The albedo of fractal stratocumulus clouds. *J. Atmos. Sci.*, **51**, 2434–2455.

Dai, A. and C. Deser: 1999, Diurnal and semidiurnal variations in global surface wind and divergence fields. *J. Geophys. Res.*, **104**, 31109–31125.

de Roode, S. R. and P. G. Duynkerke: 1997, Observed lagrangian transition of stratocumulus into cumulus during ASTEX: mean state and turbulence structure. *J. Atmos. Sci.*, **54**, 2157–2173.

de Roode, S. R., P. G. Duynkerke, and H. J. Jonker: 2004, Large eddy simulation: how large is large enough? *J. Atmos. Sci.*, **61**, 403–421.

deSzoeke, S. P. and C. S. Bretherton: 2004, Quasi-lagrangian large eddy simulations of cross-equatorial flow in the east pacific atmospheric boundary layer. *J. Atmos. Sci.*, submitted.

Fraedrich, K. and H. Bottger: 1978, A wavenumber-frequency analysis of the 500 mb geopotential at 50°*n*. *J. Atmos. Sci.*, **35**, 745–750.

Garreaud, R. D. and R. Muñoz: 2004, The diurnal cycle in circulation and cloudiness over the subtropical southeast pacific: A modeling study. *J. Clim.*, in press.

Hakim, G. J.: 2003, Developing wave packets in the north pacific storm track. *Mon. Wea. Rev.*, **131**, 342–355.

Kistler, R., E. Kalnay, W. Collins, S. Sana, G. White, J. Woolen, M. Chelliah, W. Ebisuzaki, M. Kanamitsu, V. Kousky, H. van den Dool, R. Jenne, and M. Fiorino: 2001, The ncep/ncar 50-year reanalysis. *Bull. Am. Meteorol. Soc.*, **82**, 247–267.

Klein, S. A.: 1997, Synoptic variability of low-cloud properties and meteorological parameters in the subtropical trade wind boundary layer. *J. Climate*, **10**, 2018–2039.

Klein, S. A. and D. L. Hartmann: 1993, The seasonal cycle of low stratiform clouds. *J. Climate*, **6**, 1588–1606.

Larson, V. E., R. Wood, P. R. Field, J.-C. Golaz, T. H. Vonder Haar, and W. R. Cotton: 2001, Systematic biases in the microphysics and thermodynamics of numerical models that ignore subgrid-scale variability. *J. Atmos. Sci.*, **58**, 1117–1128.

Martin, G. M., M. R. Bush, A. R. Brown, A. P. Lock, and R. N. B. Smith: 2000, A new boundary

layer mixing scheme. Part II: Tests in climate and mesoscale models. *Mon. Wea. Rev.*, **128**, 3200–3217.

Park, S., C. B. Leovy, and M. A. Rozendaal: 2004, A new single column marine boundary layer cloud model. *J. Atmos. Sci.*, submitted.

Pincus, R. and S. A. Klein: 2000, Unresolved spatial variability and microphysical process rates in large scale models. *J. Geophys. Res.*, **105**, 27059–27066.

Reynolds, R. W. and T. M. Smith: 1994, Improved global sea surface temperature analyses using optimum interpolation. *J. Clim.*, **7**, 929–948.

Rossow, W. B., C. Delo, and B. Cairns: 2002, Implications of the observed mesoscale variations of clouds for earth's radiation budget. *J. Clim.*, **15**, 557–585.

Rotstayn, L. D.: 2000, On the "tuning" of autoconversion parameterizations in climate models. *J. Geophys. Res.*, **105**, 15,495–15,507.

Rozendaal, M. A., C. B. Leovy, and S. A. Klein: 1995, An observational study of the diurnal cycle of marine stratiform cloud. *J. Clim.*, **8**, 1795–1809.

Shao, Q. and D. A. Randall: 1996, Closed mesoscale cellular convection driven by cloud-top radiative cooling. *J. Atmos. Sci.*, **53**, 2144–2165.

Slingo, J. M.: 1980, A cloud parameterization scheme derived from GATE data for use with a numerical model. *Quart. J. Roy. Meteorol. Soc.*, **106**, 774–770.

— 1987, The development and verification of a cloud prediction scheme for the ecmwf model. *Quart. J. Roy. Meteorol. Soc.*, **113**, 899–927.

Thum, N., S. K. Esbensen, D. B. Chelton, and M. J. McPhaden: 2002, Air-sea heat exchange along the northern sea surface temperature front in the eastern tropical pacific. *J. Clim.*, **23**, 3361–3378.

Wood, R. and C. S. Bretherton: 2003, Boundary layer depth, entrainment and decoupling in the cloud-capped subtropical and tropical marine boundary layer. *J. Clim.*, in press.

Wood, R., P. R. Field, and W. R. Cotton: 2002, Autoconversion rate bias in boundary layer cloud parameterizations. *Atmos. Res.*, **65**, 109–128.

Wood, R. and J. P. Taylor: 2001, Liquid water path variability in unbroken marine stratocumulus. *Quart. J. Roy. Meteorol. Soc.*, **127**, 2635–2662.

Figure Captions

Figure 1: Climatological mean value of $\overline{LWP}$ (a,b), CF (c,d), and climatological median value of γ_{LWP} (e,f) for all September/October MODIS scenes in the NE and SE Pacific.

Figure 2: Mean MBL depth for all warm cloud scenes in the NE (a) and SE (b) Pacific, Sept/Oct 2000.

Figure 3: Median values of the characteristic lengthscale for all scenes with $CF > 0.2$ for the NE (a) and SE (b) Pacific regions.

Figure 4: Fraction of MODIS scenes diagnosed as homogeneous cloud (a,b), closed MCC (c,d), and open MCC (e,f), for the NE and SE Pacific.

Figure 5: Correlation coefficient between u_{850} and $\overline{LWP}$ (a,b), CF (c,d), and γ_{LWP} (e,f), for NE (left) and SE (right) Pacific MODIS data. In this, and all subsequent regression maps, shaded areas indicate regions where the correlations are significant at the 95% level. Non-significant correlations are not contoured.

Figure 6: Correlation coefficient between lower tropospheric stability LTS and $\overline{LWP}$ (a,b), CF (c,d), and γ_{LWP} (e,f), for NE (left) and SE (right) Pacific MODIS data.

Figure 7: Correlation coefficient between temperature advection and $\overline{LWP}$ (a,b), CF (c,d), and γ_{LWP} (e,f), for NE (left) and SE (right) Pacific MODIS data.

Figure 8: Cloud fraction (a,b) and LTS (c,d) standard deviation in the NE and SE Pacific.

Figure 9: Correlation coefficient between MBL depth and $\overline{LWP}$ (a,b), CF (c,d), and γ_{LWP} (e,f), for NE (left) and SE (right) Pacific MODIS data.

Figure 10: Correlation coefficient between MBL depth and LTS for NE (a) and SE (b) Pacific data.

Figure 11: Dominant timescales for modulation of cloud structural parameters (a) and large scale forcings (b), plotted as a function of latitude for the NE and SE Pacific regions. Error bars show the 2-σ estimated uncertainty in the mean timescale, estimated using the available $5\times5^\circ$ grid-box data at each latitude.

Figure 12: Mean values of 850 hPa vertical wind w_{850} (a,b), LTS (c,d), and temperature advection $\mathbf{U}\cdot\nabla SST$ (e,f) for the corresponding MODIS scenes in the NE (left) and SE (right) Pacific during September/October 2000.

Figure 13: (a) Two-monthly mean values of MODIS scene cloud fraction as a function of LTS. Each point represents a single $2.5\times2.5^\circ$ region. The dotted line shows the results of Klein and Hartmann (1993) and the dashed line the best fit to the MODIS data for the NE and SE Pacific.

(b) Cloud fraction as a function of MODIS-derived MBL depth.

Figure 14: Median characteristic cell lengthscale λ_1 binned by MBL depth z_i for all MODIS scenes (solid circles) over the NE and SE Pacific. The dotted lines denote aspect ratios of 20:1, 30:1 and 40:1. Error bars indicate the approximate sampling error in the median. The solid line indicates the fit described in the text.

Figure 15: Standard deviations of liquid water path σ_{LWP} (a,b) and saturation excess σ_s (c,d) plotted against cell scale λ_1 (a,c) and z_i (b,d). MODIS data are shown using solid (NE Pacific) and open (SE Pacific) circles, which represent median values for binned z_i ranges, with dashed and dotted lines respectively indicating 25th and 75th percentiles. Also shown are results from FIRE, EPIC and ASTEX (see text). The gray dashed lines in (b) and (d) are parameterizations described in the text.

Figure 16: Schematic figure showing the evolution of the MBL from the near coastal regions containing stratus to the NE of the subtropical high, through the stratocumulus regions where MCC initiates, to the trade wind regions dominated by clusters of cumulus clouds detraining stratiform cloud at the top of the MBL. The shaded region denotes the pdf of the LCL (cloud base height) which increases in both mean and variance downwind. The fraction of the pdf where $LCL < z_i$ contains cloud. This evolution of the LCL pdf (or equivalently the saturation deficit pdf) provides a theoretical framework for the observed changes in the mesoscale variability of clouds in the subtropics.

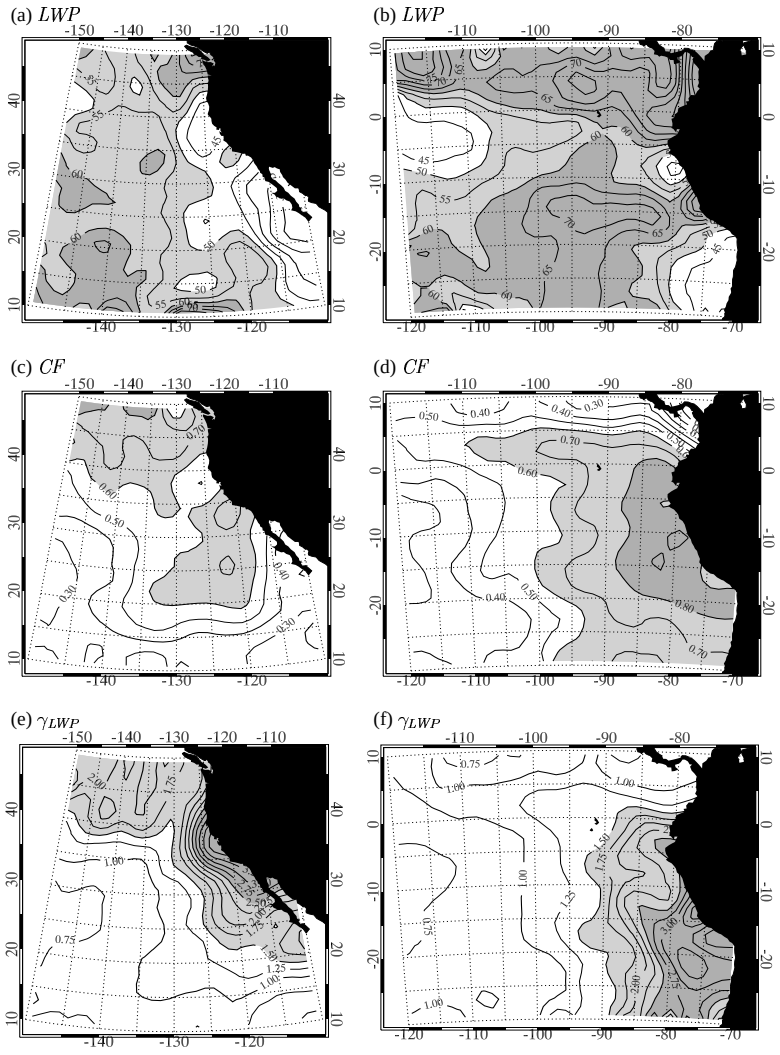

Figure 1:

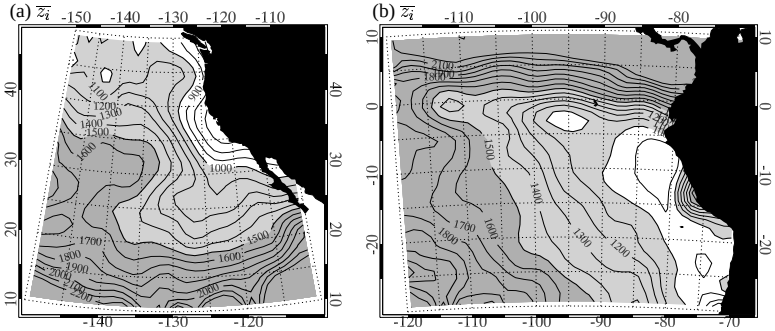

Figure 2:

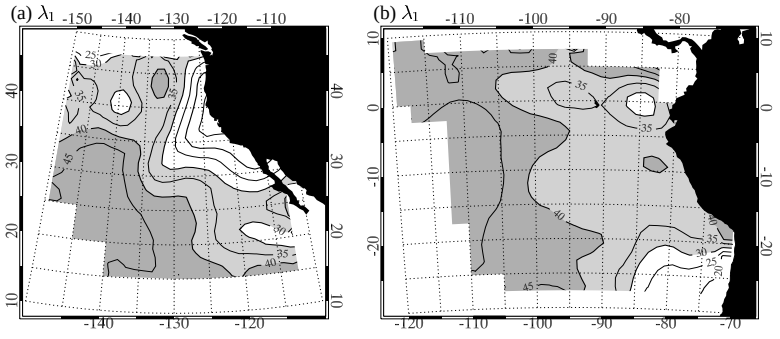

Figure 3:

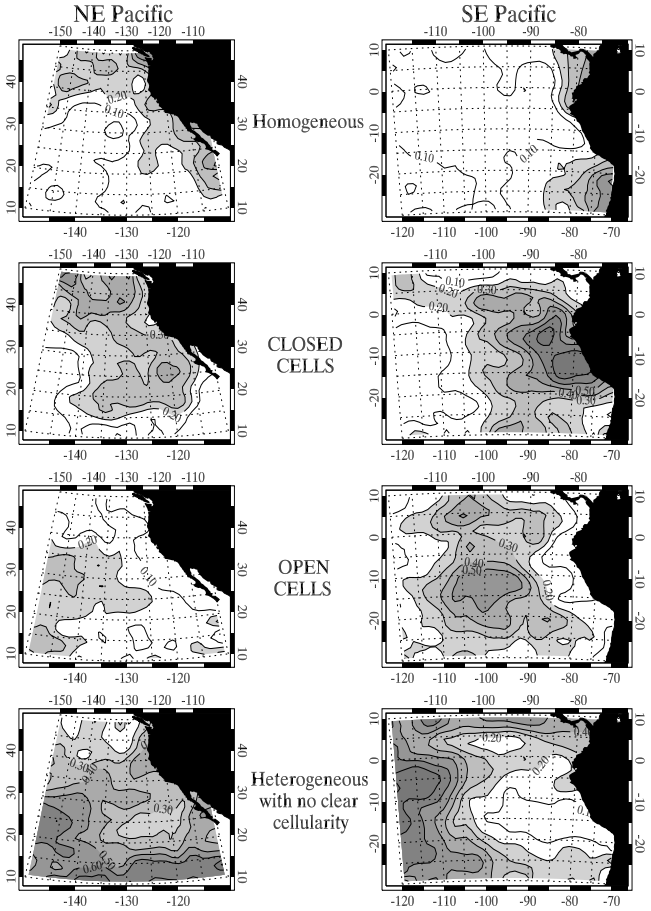

Figure 4:

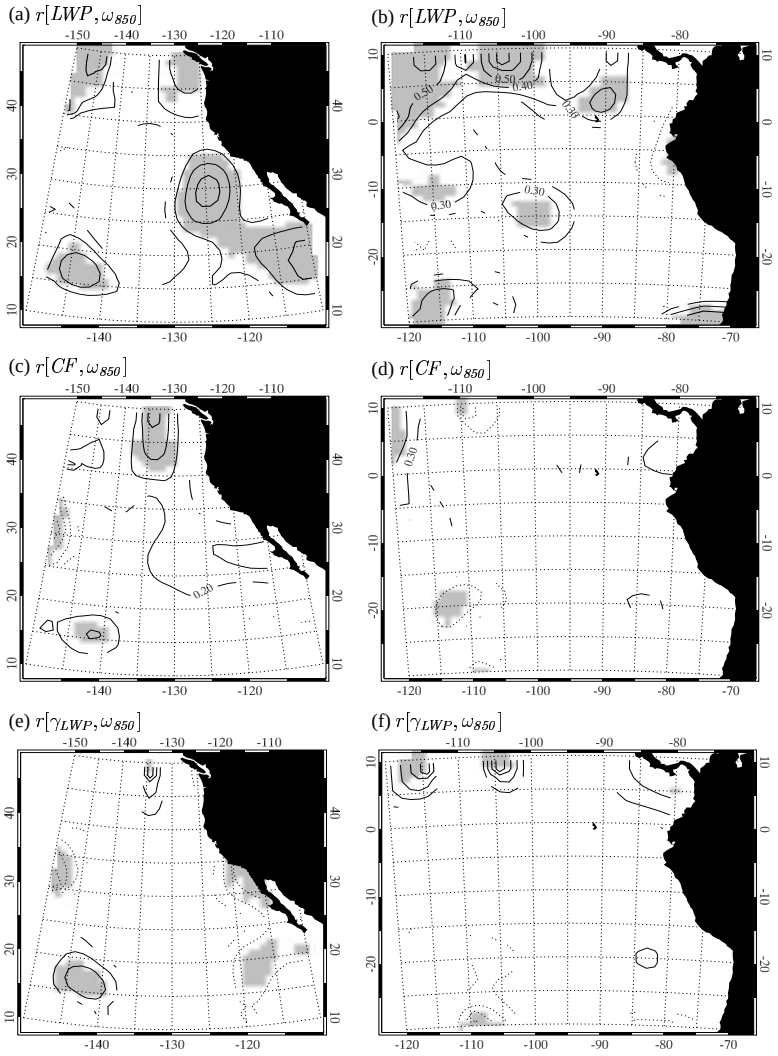

Figure 5:

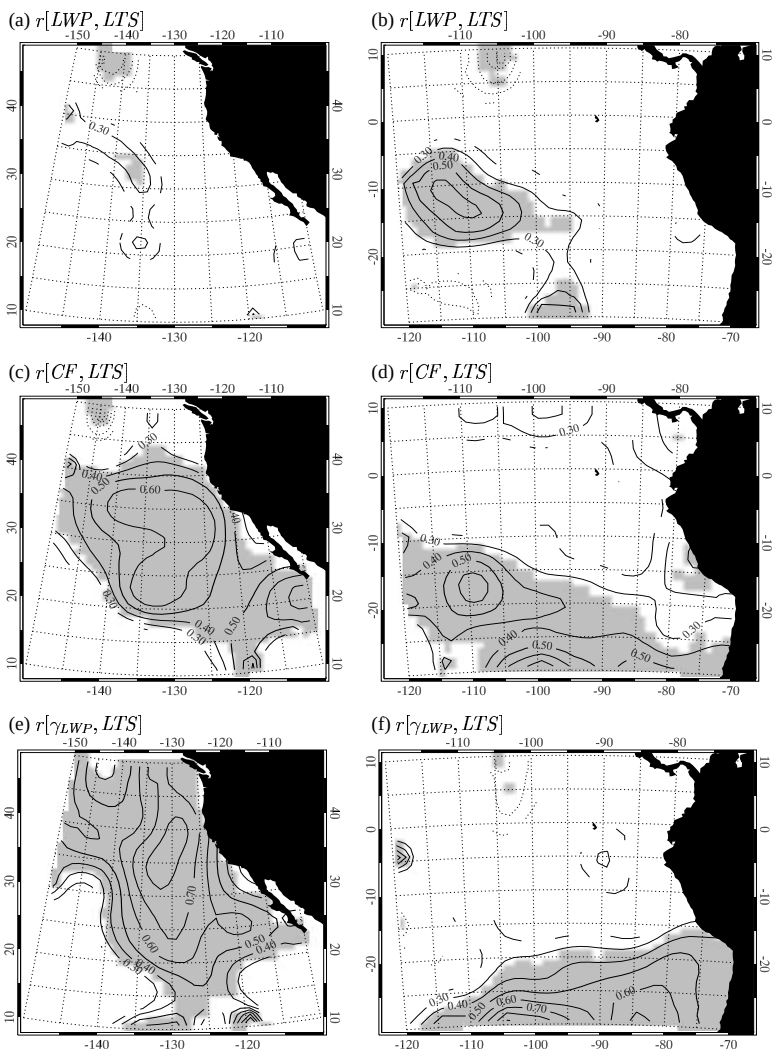

Figure 6:

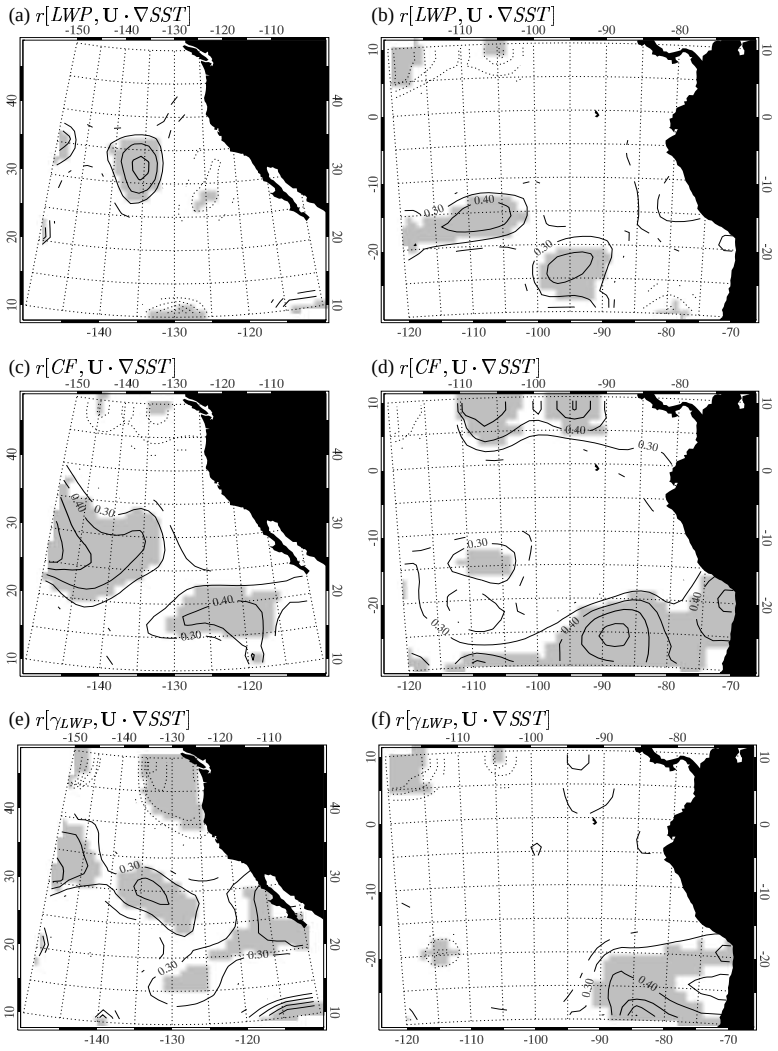

Figure 7:

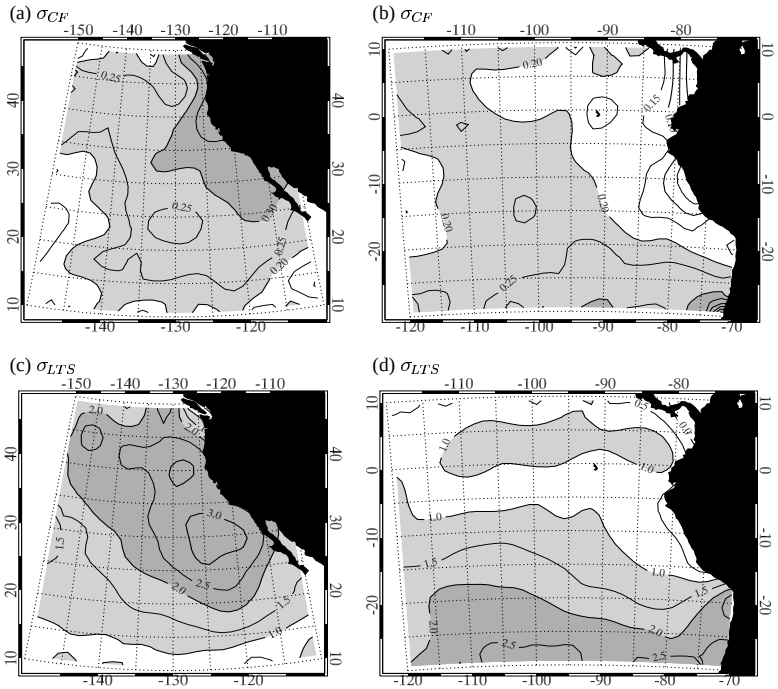

Figure 8:

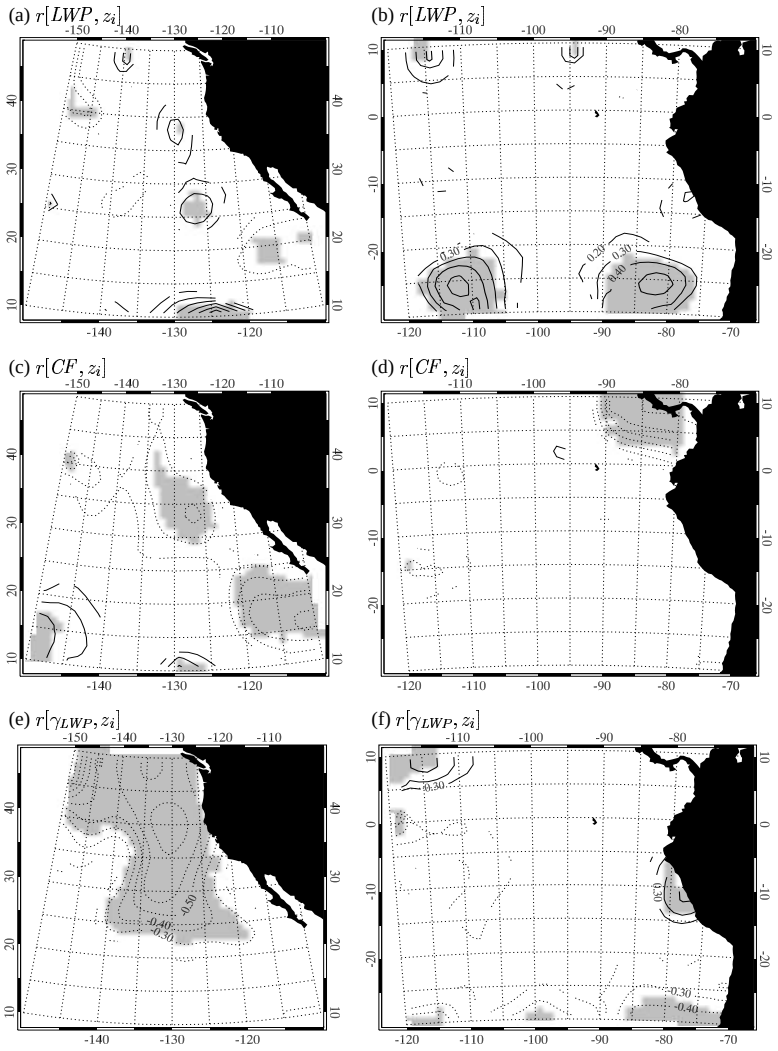

Figure 9:

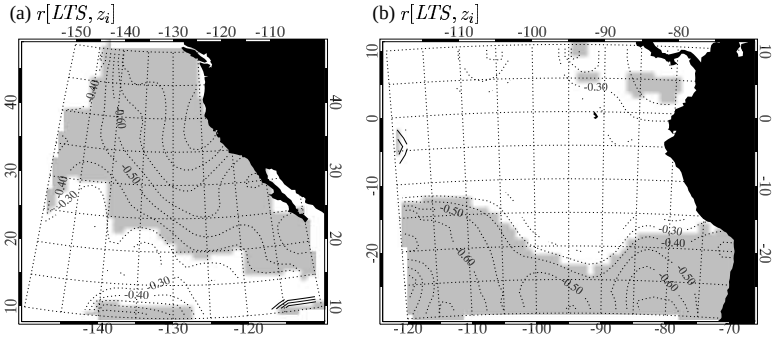

Figure 10:

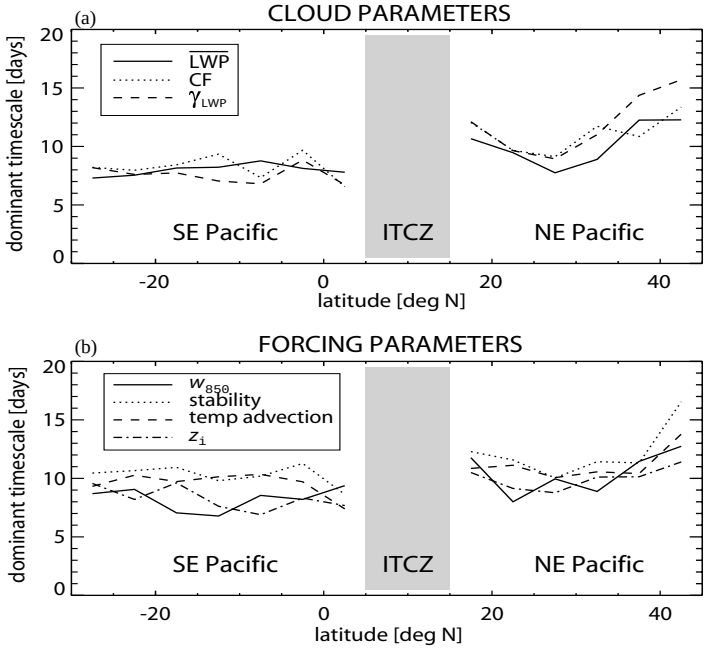

Figure 11:

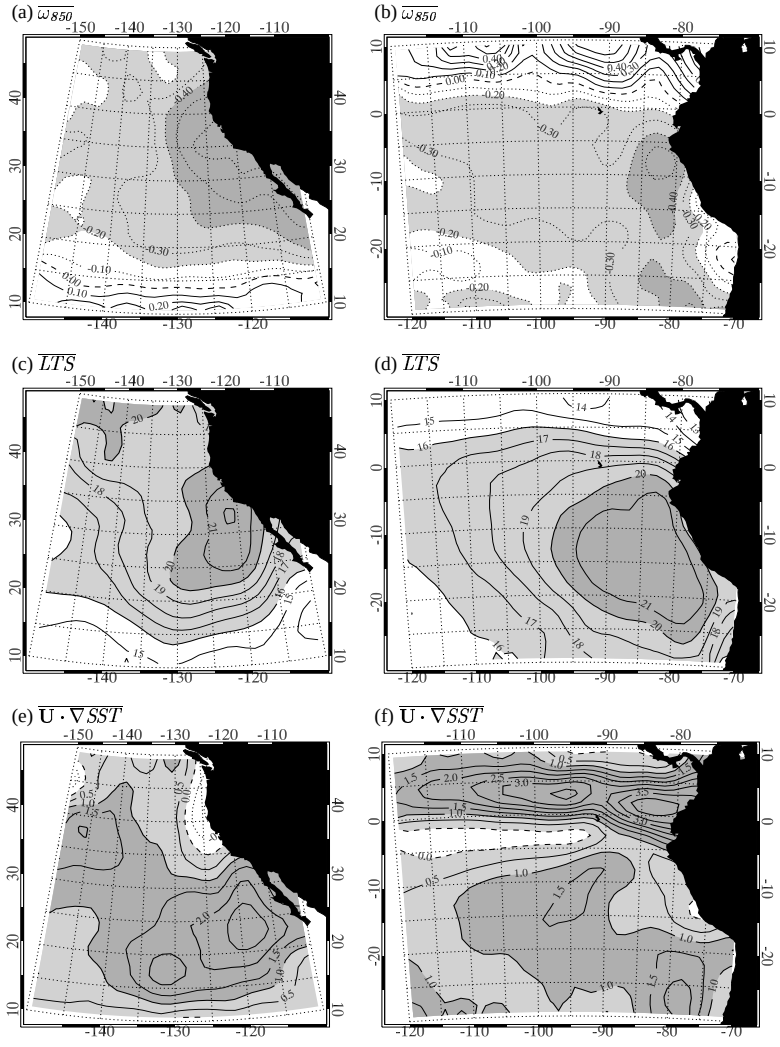

Figure 12:

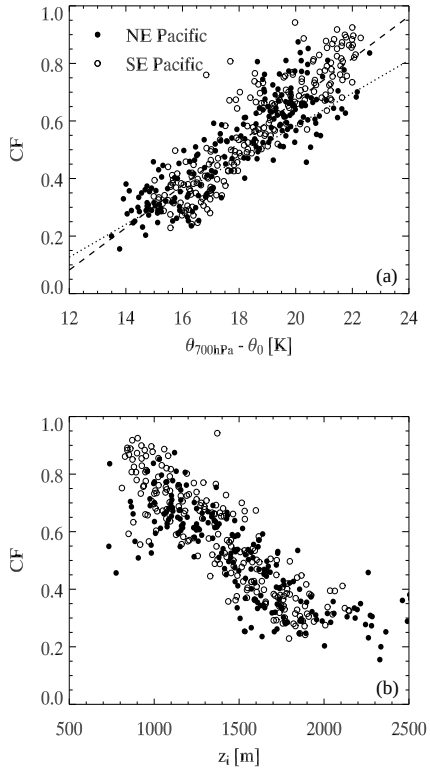

Figure 13:

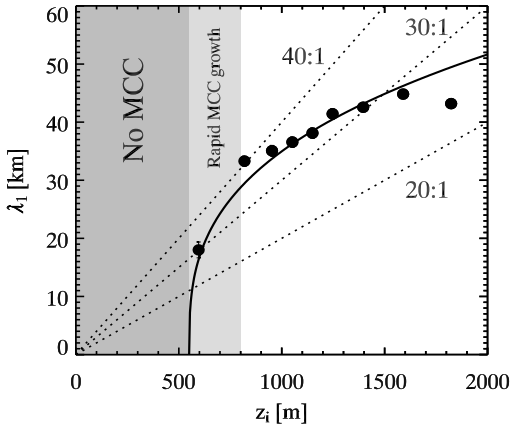

Figure 14:

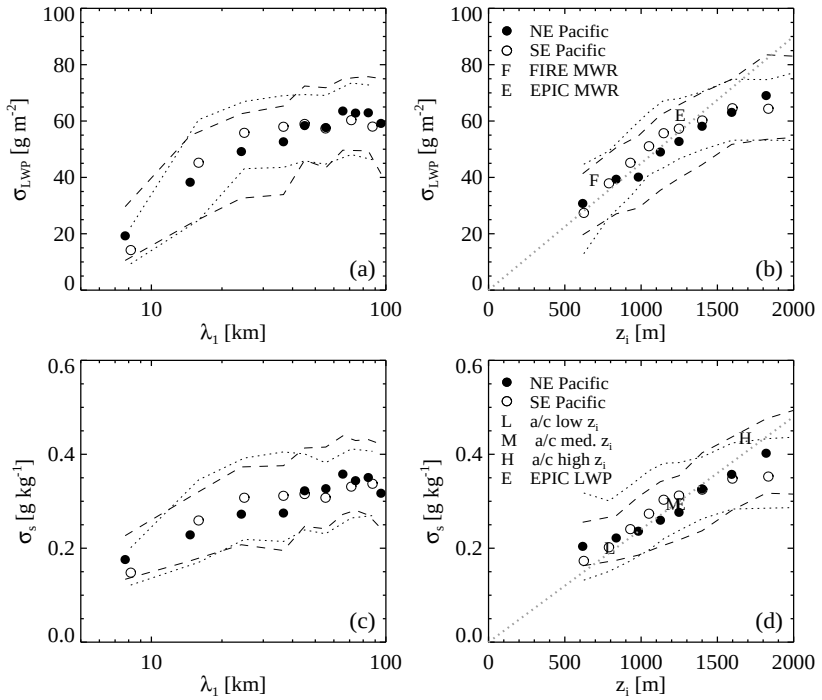

Figure 15:

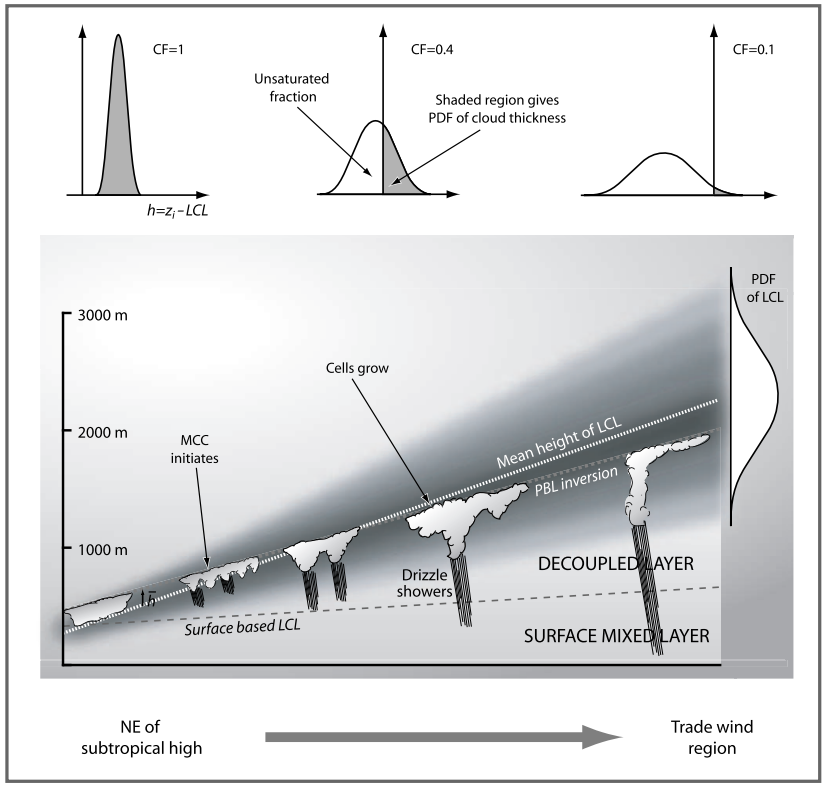

Figure 16: